Bioactive Materials 10 (2022) 420–429

Contents lists available at ScienceDirect

Bioactive Materials

journal homepage: www.sciencedirect.com/journal/bioactive-materials

Drug-peptide supramolecular hydrogel boosting transcorneal permeability and pharmacological activity via ligand-receptor interaction

Lin Chen [a], Jie Deng [b,1], Ailing Yu [a,1], Yuhan Hu [a], Bo Jin [a], Pengyuan Du [a], Jianhong Zhou [a], Lei Lei [a], Yuan Wang [a], Serhii Vakal [c], Xingyi Li [a,*]

[a] Institute of Biomedical Engineering, School of Ophthalmology & Optometry, Eye Hospital, Wenzhou Medical University, 270 Xueyuan Road, Wenzhou, 325027, PR China
[b] Key Laboratory of Diagnosis and Treatment of Severe Hepato-Pancreatic Diseases of Zhejiang Province, The First Affiliated Hospital, Wenzhou Medical University, Wenzhou, 325027, PR China
[c] Structural Bioinformatics Laboratory, Biochemistry, Åbo Akademi University, Turku, 20541, Finland

ARTICLE INFO

Keywords:
Active transport
Integrin
Supramolecular hydrogel
Ocular retention
Corneal permeability

ABSTRACT

Boosting transcorneal permeability and pharmacological activity of drug poses a great challenge in the field of ocular drug delivery. In the present study, we propose a drug-peptide supramolecular hydrogel based on anti-inflammatory drug, dexamethasone (Dex), and Arg-Gly-Asp (RGD) motif for boosting transcorneal permeability and pharmacological activity via the ligand-receptor interaction. The drug-peptide (Dex-SA-RGD/RGE) supramolecular hydrogel comprised of uniform nanotube architecture formed spontaneously in phosphate buffered saline (PBS, pH = 7.4) without external stimuli. Upon storage at 4 °C, 25 °C, and 37 °C for 70 days, Dex-SA-RGD in hydrogel did not undergo significant hydrolysis, suggesting great long-term stability. In comparison to Dex-SA-RGE, Dex-SA-RGD exhibited a more potent *in vitro* anti-inflammatory efficacy in lipopolysaccharide (LPS)-activated RAW 264.7 macrophages via the inhibition of nuclear factor κB (NF-κB) signal pathway. More importantly, using drug-peptide supramolecular hydrogel labeled with 7-nitro-2,1,3-benzoxadiazole (NBD), the Dex-SA-K(NBD)RGD showed increased performance in terms of integrin targeting and cellular uptake compared to Dex-SA-K(NBD)RGE, as revealed by cellular uptake assay. On topical instillation in rabbit's eye, the proposed Dex-SA-K(NBD)RGD could effectively enhance the transcorneal distribution and permeability with respect to the Dex-SA-K(NBD)RGE. Overall, our findings demonstrate the performance of the ligand-receptor interaction for boosting transcorneal permeability and pharmacological activity of drug.

1. Introduction

A number of ocular diseases, including diabetic retinopathy, cataract, uveitis, and glaucoma, significantly impair the patient's vision and thus affect the quality of life worldwide [1–3]. Until now, eye drops in the forms of solution and hydrogel are still the dominant formulation for the ocular administration to treat various ocular diseases. However, due to the existence of several inherent anatomical and physiological barriers (*e.g.,* corneal barrier, blood-aqueous humor barrier, blood-retinal barrier), the foreign substances, including drugs, can hardly across these barriers to reach the lesion site [4–7]. Additionally, tears continuously flush the ocular surface before draining into the nasolacrimal duct, and the eyelid blinking wipes and clean the ocular surface from debris and excess fluids, thus leading to quick removal of drugs [8–10]. Therefore, the ocular bioavailability of topically administrated drugs is generally less than 5%, often requiring multiple administrations daily to maintain its minimal therapeutic drug concentration [11]. As the frequency of daily administration of eye-drops increases, the potential risk of ocular irritation and systemic side effects increase accordingly. Hence, the more efficient and longer-lasting topical ocular drug delivery is still an unmet ophthalmic need.

To enhance ocular bioavailability without compromising the disruption of the corneal epithelium, the eye-drop formulation should provide high concentration of a soluble drug after topical instillation as

Peer review under responsibility of KeAi Communications Co., Ltd.
* Corresponding author. School of Ophthalmology & Optometry and Eye Hospital, Wenzhou Medical University, 270 Xueyuan Road, PR China.
E-mail addresses: lixingyi_1984@mail.eye.ac.cn, lixingyi_1984@mail.eye.ac.cn (X. Li).
[1] Jie Deng and Ailing Yu did equal work with Lin Chen, so they should be treated as co-first authors for this paper.

https://doi.org/10.1016/j.bioactmat.2021.09.006
Received 27 July 2021; Received in revised form 4 September 2021; Accepted 5 September 2021
Available online 10 September 2021

long as possible. Over the past several decades, various formulation-based strategies aimed at extending the precorneal retention or enhancing corneal permeability have been developed and tested *in vitro* and *in vivo* [12–14]. These strategies utilize chemical penetration enhancers, prodrugs, penetrating peptides, and drug delivery vehicles such as liposomes and micro/nanoparticles to improve drug corneal permeability [15–19]. Another alternative is polymeric gel forming systems, which undergo a sol-gel transition triggered by temperature, ions, or some other physical stimuli upon application to the eye, thus providing a long-term precorneal retention and enhancing corneal permeability [12,20–23]. They allow encapsulation of several therapeutic agents to achieve the desired therapeutic outcomes, and some of them (*e.g.,* carbomer, gellan gum) have been clinically launched [24,25]. Although significant achievements have been reached, the rapid gelation upon contact with the ocular surface typically leads to clumpy gels that can also be messy and cause blurred vision.

Nowadays, a drug-peptide supramolecular hydrogel formed spontaneously by amphiphilic drug-peptide conjugates represents an important class of therapeutic strategies [26,27]. In contrast to their polymer-based counterparts, this type of hydrogel offers several advantages, such as inherent biodegradability and biocompatibility, precise and relatively high drug payload, minimal gelation concentration and thixotropy [26,28–32]. Meanwhile, the utilization of peptides confers a great degree of functionality to a hydrogel and allows active targeting of a particular receptor on the desired cells. Given that several integrins are widely expressed on all nucleated cells including corneal epithelial cells, phagocytic cells [33–36], we rationally designed and synthesized an integrin-targeted drug-peptide conjugate based on Arg-Gly-Asp (RGD) motif. This drug-peptide conjugate formed supramolecular hydrogel spontaneously in phosphate buffered saline (PBS; pH = 7.4) without external stimuli, endowing its great applicability for topical ocular drug delivery. The concept of our formulation approach is that the topical ocular administration of a peptide-drug supramolecular hydrogel could not only provide the extended ocular drug delivery via the resistance of the tear elimination, simultaneously enhanced drug transcorneal permeability and pharmacological activities by the ligand-receptor interaction between integrin expressed in the targeted cells (*i.e.,* corneal epithelial cell, macrophage) and RGD motif in supramolecular hydrogel (Scheme 1). To the best of our knowledge, this is the first report on the usage of RGD-based prodrug supramolecular hydrogel for boosting transcorneal permeability and pharmacological activity via the ligand-receptor interaction.

2. Materials and methods

2.1. Materials

Dexamethasone (Dex) was purchased from Dalian Meilun Biology Technology Co., Ltd. (Dalian, China). Succinic anhydride (SA) was purchased from J&K Scientific Ltd. (Beijing, China). Succinated Dex (Dex-SA) was synthesized using a method described in our previous study [15]. The 2-chlorotrityl chloride resin and N-Fmoc-protected amino acids were provided by GL Biochem Ltd. (Shanghai, China). Pyrene was purchased from Alfa Aesar (USA). 4-Chloro-7-nitrobenzofurazan (NBD-Cl), porcine liver esterase, thiazolyl blue tetrazolium bromide (MTT), lipopolysaccharide (LPS), Griess reagent, insulin, and epidermal growth factor (EGF) were provided by Sigma-Aldrich (USA). Fetal bovine serum (FBS) was obtained from Gibco (USA). DMEM, penicillin-streptomycin, bicinchoninic acid (BCA) assay kit, and enhanced chemiluminescence reagent were supplied by Thermo Fisher Scientific (USA). Mouse TNF-α DuoSet ELISA (DY410-15) and mouse IL-6 DuoSet ELISA (DY406-15) were obtained from R&D Systems®

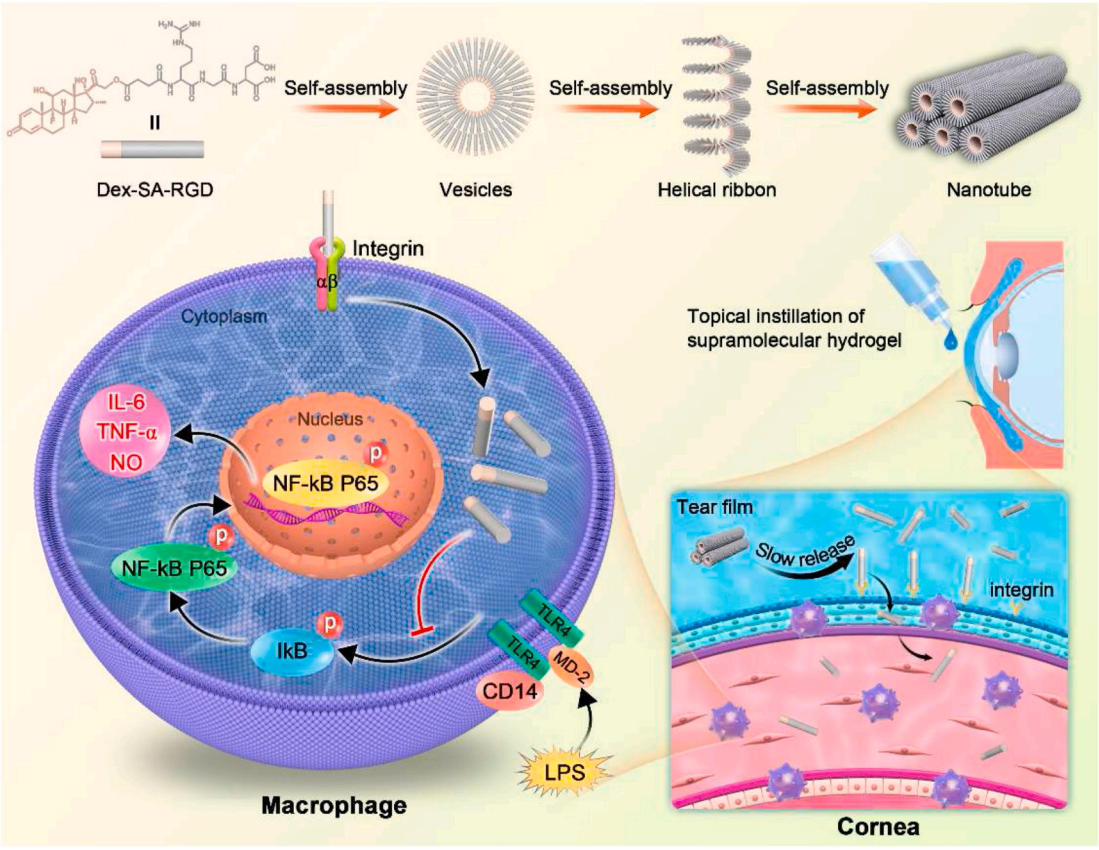

Scheme 1. Self-assembly of Dex-SA-RGD into a supramolecular hydrogel and a schematic illustration of a ligand-receptor interaction strategy for boosting drug transcorneal permeability and pharmacological activity.

(USA). RIPA lysis buffer, Triton X-100, and bovine serum albumin (BSA) were purchased from Solarbio (Beijing, China). Phosphatase and protease inhibitor cocktail were supplied by Biomake (USA). Polyvinylidene difluoride (PVDF) membrane was purchased from Millipore (USA). The primary antibodies against p65, p-p65, IκB, p-IκB and horseradish peroxidase-labeled secondary antibody were obtained from Cell Signaling Technology (USA). The primary antibody against GAPDH and FITC-conjugated secondary antibody were purchased from Proteintech (Wuhan, China). 4% paraformaldehyde and DAPI were obtained from Beyotime (Shanghai, China). Anti-fluorescence quenching mounting tablets were provided by Biosharp (Hefei, China). Artificial tears (Systane Ultra Lubricant Eye Drops) were purchased from Alcon Research LLC. All other reagents were of analytical grade.

2.2. Synthesis of drug-peptide conjugate

Briefly, the Dex-SA-RGD and Dex-SA-RGE conjugates were synthesized by a classic solid-phase peptide synthesis (SPPS) method using 2-chlorotrityl chloride resin and N-Fmoc-protected amino acids. The 2-chlorotrityl chloride resin (1 g) was first swelled in dry dichloromethane (DCM) for 15 min, and then the first amino acid was loaded onto the resin, as a solution of Fmoc-protected amino acid and N,*N*-diisopropylethylamine (DIEA; 2 equiv) in DCM, for 1 h. After washing the column 5 times with DCM, the unreactive sites of the resin were blocked for 10 min with a blocking solution (DIEA:DCM:MeOH = 1:17:2; v/v/v). The Fmoc protective group was then removed by the addition of 20% piperidine in DMF, followed by coupling the Fmoc-protected amino acid to the free amino group on the resin using DIEA (2 equiv) and O-benzotriazol-1-yl-tetramethyluronium hexafluorophosphate (HBTU) (1 equiv) as the coupling agent in DMF for 2 h. These two steps were repeated to elongate the peptide chain. Finally, Dex-SA was coupled to the peptide by adding DIEA (2 equiv) and HBTU (1 equiv) in DMF for 2 h. The resulting Dex-SA-RGD and Dex-SA-RGE conjugates were cleaved from the resin with a washing solution (TFA: TIS:H_2O = 95:2.5:2.5; v/v/v). The obtained crude product was purified by reversed-phase high-performance liquid chromatography (HPLC) and characterized by mass spectrometry (MS), and lyophilized for further use.

To obtain Fmoc-K(NBD), anhydrous sodium carbonate (1.06 g; 10 mmol) was dissolved in 30 mL of distilled water, followed by the addition of 30 mL of Fmoc-Lys-OH (1.84 g; 5 mmol) methanol solution with the aid of the ultrasound. After that, 30 mL of NBD-Cl (1.2 g; 6 mmol) methanol solution were added to react at room temperature overnight. The resulting mixture was extracted with hexane/ethyl acetate (5:1; v/v), and the extracts were collected by the addition of 1 N hydrochloric acid to afford precipitates. After filtration, the residual solution was extracted with ethyl acetate several times, and the organic phase was collected and dried by rotary evaporation to obtain Fmoc-K(NBD)-OH. Finally, the Dex-SA-K(NBD)RGD and Dex-SA-K(NBD)RGE conjugates were synthesized by an SPPS method as described above.

2.3. Preparation of a drug-peptide supramolecular hydrogel

An indicated amount of the Dex-SA-RGD and Dex-SA-RGE conjugates were suspended into phosphate buffered saline (PBS, pH = 7.4) under vortexing. The hydrogelation was monitored by the inverted tube test as reported previously [37].

2.4. Characterization

2.4.1. Critical aggregate concentration (CAC)

The CAC values of Dex-SA-RGD and Dex-SA-RGE conjugates were measured by dynamic light scattering (DLS) [38]. Aqueous solutions containing different concentrations of Dex-SA-RGD and Dex-SA-RGE conjugates were used for the test, and the light scattering intensity as a function of concentration was recorded and analyzed using Origin software.

2.4.2. Circular dichroism (CD) spectroscopy

The tested samples were placed into a quartz spectrophotometer cell and measured by a BioLogic (MOS-450) system. Absorption spectra have been collected as HT voltage and converted into absorbance in a range of 180–300 nm. The resultant CD spectra were acquired after subtracting the solvent background.

2.4.3. Transmission electron microscopy (TEM)

A negative staining technique was used to observe the microstructural images from solution or hydrogels using transmission electron microscopy (F200S, FEI, USA). Samples were pipetted onto a copper grid and washed by distilled water three times, followed by negative staining with 0.5 wt% phosphotungstic acid and then air-dried in a desiccator overnight before the observation.

2.4.4. Rheology

The rheological properties of Dex-SA-RGD and Dex-SA-RGE supramolecular hydrogels were measured by a rheometer (AR2000, TA instrument, USA) using a 40-mm cone-plate. A portion (0.5 mL) of tested samples was loaded, and a frequency sweep from 0.1 to 100 rad/s was conducted at 25 °C with a strain of 1%. A strain sweep was performed at 25 °C at a constant frequency of 1 Hz. A strain amplitude sweep with a strain of 1% and 100% was performed at 25 °C at a constant frequency of 1 Hz. A temperature sweep from 25 to 55 °C was performed with a strain of 1%.

2.4.5. Stability test

To explore the stability of Dex-SA-RGD in a hydrogel, we traced the hydrolysis of Dex-SA-RGD using high-performance liquid chromatography (HPLC; Agilent 1290). The hydrogels were stored at 4 °C, 25 °C, and 37 °C for 70 days under a sealed condition. At specific time points, hydrogels were collected, and hydrogel components were analyzed by HPLC (ZORBAX Eclipse XDB-C18, 150 mm × 4.6 mm i.d., 5 μm, Agilent, USA). The mobile phase was composed of acetonitrile and 0.1% triethylamine phosphate solution (60/40; v/v) at a flow rate of 1.0 mL/min. The eluate was detected at 240 nm using a DAD detector.

2.5. In vitro release study

The *in vitro* drug release behavior of Dex-SA-RGD and Dex-SA-RGE hydrogels was performed in phosphate buffered saline (PBS, pH = 7.4) at 37 °C. In brief, 0.2 mL of Dex-SA-RGD or Dex-SA-RGE hydrogels were pre-formed in a 5 mL Eppendorf (EP) tube to give a final Dex-SA-RGD or Dex-SA-RGE concentration at 20 mg/mL. And then, 2 mL of PBS was added as a release medium for a period of *in vitro* release study. At predetermined time points, 1 mL of release medium was withdrawn for the quantification of released drugs in terms of Dex and Dex-SA-RGD/Dex-SA-RGE by an HPLC assay as described above, and an additional 1 mL of freshly prepared PBS was added at each time interval for continuous study.

2.6. In vitro gel dissolution in artificial tears

In brief, 0.5 mL Dex-SA-RGD hydrogel (20 mg/mL) pre-formed in a glass bottles and weighted. After resting for 30min, 0.5 mL artificial tears was added to each bottles and placed into an air bath (37 ± 0.2 °C) with a constant shaking (40 rpm) for a period of *in vitro* gel dissolution test. At specific time intervals, the culture artificial tears from each bottle were discarded carefully and the residues were weighted. At each time interval, 0.5 mL freshly artificial tears was added into each bottle for continuous study. The *in vitro* gel dissolution ratio in artificial tears were expressed as the cumulative dissolved gels as function with time. The experiment was repeated three times.

2.7. In vitro cytotoxicity test

The *in vitro* cytotoxicity of the Dex-SA-RGD and Dex-SA-RGE hydrogels to the human corneal epithelial cells (HCEC) and RAW 264.7 macrophages was evaluated using the MTT assay. HCEC were cultured in DMEM/F12 with 10% Fetal Bovine Serum (FBS), 1% Penicillin-Streptomycin (Pen Strep), 0.2% Insulin, and 0.0005% HEGF. RAW 264.7 macrophages were cultured in DMEM with 10% FBS and 1% Pen Strep. In brief, HCEC and RAW 264.7 cells were seeded in a 96-well plate at a density of 1×10^4 cells/well with 100 μL of cell culture medium and incubated overnight in a CO_2 incubator at 37 °C. After that, a series of Dex-SA-RGD and Dex-SA-RGE hydrogels with concentrations in the range of 0–500 μM were added to each well for co-incubation. After 24 h of incubation, 20 μL of MTT solution were added to each well for another 4 h of incubation, followed by the addition of DMSO to dissolve the formed formazan. The absorbance was recorded at a wavelength of 570 nm with a microplate reader (Model SpectraMax M5, Molecular Devices, USA). The untreated cells were used as a control. The cell viability was determined using the following equation: Cell viability (%) = absorbance of the tested sample/absorbance of the control sample × 100%.

2.8. Nitric oxide (NO) measurement

NO levels in the culture supernatants was measured by Griess assay. RAW 264.7 macrophages at a density of 2×10^5 cells/well were seeded in a 24-well plate and incubated overnight. Cells were pre-treated with 200 nM Dex-SA-RGD or Dex-SA-RGE for 2 h, followed by stimulation with 1 μg/mL LPS for 24 h. After that, the mixture of 100 μL supernatant and 100 μL Griess reagent were added to a 96-well plate and incubated for 15 min. The absorbance at 540 nm was recorded using a microplate reader (Model SpectraMax M5, Molecular Devices, USA).

2.9. Enzyme-linked immunosorbent assay (ELISA)

RAW 264.7 macrophages at a density of 2×10^5 cells/well were seeded in a 24-well plate and cultured overnight. Cells were pre-treated with 200 nM Dex-SA-RGD or Dex-SA-RGE for 2 h, followed by stimulation with 1 μg/mL LPS for 24 h. Thereafter, the secreted IL-6 and TNF-α levels in the culture medium were measured by ELISA kits based on the manufacturer's procedure.

2.10. Western blotting

RAW 264.7 macrophages at a density of 5×10^5 cells/well were seeded in a 6-well plate and cultured overnight. Cells were pre-treated with 200 nM Dex-SA-RGD or Dex-SA-RGE for 2 h, followed by stimulation with 1 μg/mL LPS for 24 h. After that, cells lysate were obtained in RIPA lysis buffer containing 1 × phosphatase inhibitor cocktail and protease inhibitor cocktail. The protein extractions were quantified using a bicinchoninic acid (BCA) assay kit. 20 μg protein of each sample was separated by sodium dodecyl sulfate-polyacrylamide gel electrophoresis (SDS-PAGE, 12%) and transferred to polyvinylidene difluoride (PVDF) membrane. After blocking with 10% skim milk in TBST at room temperature for 2 h, the primary antibodies against p65 (1:1000), p-p65 (1:1000), IκB (1:1000), p-IκB (1:1000) and GAPDH (1:10000) were probed with membranes overnight at 4 °C, followed by the addition of horseradish peroxidase-labeled secondary antibody (1:1000) for 1 h incubation at room temperature. Enhanced chemiluminescence assay was used to visualize the immunoreactive bands on Amersham Imager 680 (GE, USA). The bands optical density were quantified using ImageJ software (Version 1.8.0, USA).

2.11. Immunofluorescence (IF)

RAW 264.7 macrophages at a density of 1×10^4 cells/well were seeded into a 12-well chamber slide and cultured overnight. Cells were pre-treated with 200 nM Dex-SA-RGD or Dex-SA-RGE for 2 h, followed by stimulation with 1 μg/mL LPS for 24 h. Subsequently, cells were fixed with 4% paraformaldehyde for 30 min and permeabilized with 0.1% Triton X-100 for 10 min. After blocking with 3% bovine serum albumin (BSA) for 1 h, cells were probed with p65 (1:100) overnight at 4 °C, followed by the incubation of FITC-conjugated secondary antibody (1:400) for an additional hour in the darkness at room temperature. Nuclear stain was performed with DAPI. Images were acquired using Leica SP8 confocal microscope (Leitz Aristoplan, Germany) with 40 × objective. The images were processed employing Image J software (Version 1.8.0, USA).

2.12. Cellular uptake assay

HCEC were used to assess cellular uptake of Dex-SA-K(NBD)-RGD and Dex-SA-K(NBD)-RGE. In brief, a round glass sheet was laid on the bottom of a 24-well plate, and HCEC were seeded in 24-well plate at a density of 5×10^4 cells/well and incubated overnight in a 5% CO_2 incubator at 37 °C. After 24 h of incubation, the cells were treated with 500 μM Dex-SA-K(NBD)RGD or Dex-SA-K(NBD)RGE for 0.5 and 2 h, respectively. After washing with phosphate buffered saline (PBS; pH = 7.4) three times, the cells were fixed with 4% paraformaldehyde for 20 min and then stained with DAPI for 3–5 min at 37 °C. Finally, fluorescence signal was observed with a confocal microscope (LSM 710, ZEISS, Germany). Additionally, the cells were pre-treated by 500 μM Dex-SA-RGD for 2 h to block integrin, and then incubated with 500 μM Dex-SA-K(NBD)RGD for 0.5 and 2 h to visualize the changes of fluorescence intensity.

2.13. In vivo distribution test

All experimental protocols were approved by the Institutional Animal Care and Use Committee of Wenzhou Medical University. New Zealand white rabbits (2–2.5 kg) were used for *in vivo* distribution test. To assess the *in vivo* distribution of Dex-SA-K(NBD)RGD and Dex-SA-K(NBD)RGE in the rabbit eye after a single topical instillation, a fluorescence microscope (DM4B, LEICA, Germany) was employed. In brief, 50 μL of either Dex-SA-K(NBD)RGD or Dex-SA-K(NBD)RGE (20 mg/mL) aqueous solution were instilled into the underconjunctival sac of each rabbit's eye. After 15 and 45 min of instillation, the rabbits were sacrificed, and the eyeballs were excised. Finally, the corneal cryostat sections were prepared and imaged to visualize the green fluorescence distributed in the tissue with a fluorescence microscope (DM4B, LEICA, Germany).

2.14. Statistical analysis

In all experiments, the measured values were expressed as the mean ± SD and statistically analyzed with Origin 7.5 (Origin Lab, USA). *In vitro* cytotoxicity data and *in vitro* anti-inflammatory efficacy data were analyzed by one-way analysis of variance (ANOVA) with Tukey's multiple comparisons test using GraphPad Prism 7.00 (GraphPad Software, USA). Statistical significance was considered at a probability level of $P < 0.05$.

3. Results and discussion

3.1. Drug-peptide conjugate design and hydrogelation

As proved previously, integrins, acting as receptors for extracellular matrix (ECM) proteins, are expressed on all nucleated cells (*i.e.,* corneal epithelial cells, phagocytic cells) [34–36]. As a ligand for integrins, fibronectin is primarily localized to the ECM, and the ligand-receptor interaction results in the activation of various intracellular signaling pathways that play vital roles in many biological processes involving cell

adhesion, detachment, differentiation, proliferation, and migration [33,34,39–41]. The major integrin-binding site of fibronectin is the amino acid sequence Arg-Gly-Asp (RGD) in the 10th type III domain. Indeed, various types of biomaterials based on the RGD motif have been developed and shown to support cell adhesion, migration, and proliferation of epithelial cells for the application in corneal wound healing [42–45]. Inspired by that, we suggested that the utilization of ligand-receptor interaction between fibronectin's RGD motif and integrin to formulate an ophthalmic drug delivery system is expected to boost transcorneal permeability and pharmacological activity. Herein, we reported the design of Dex-SA-RGD as a hydrogelator, which can spontaneously self-assemble into supramolecular hydrogel with potential for the enhanced ocular drug delivery via receptor-ligand interaction. Briefly, Dex-SA-RGD/Dex-SA-RGE and Dex-SA-K(NBD) RGD/Dex-SA-K(NBD)RGE conjugate was synthesized, followed by a purification to 95% homogeneity by reversed-phase HPLC. The identity and purity of both components was further identified using LC-MS (Figs. S1–2). The structures of the resulting Dex-SA-RGD and Dex-SA-RGE are shown in Fig. 1A. To identify the hydrogelation of these two compounds, we dissolved the indicated amounts of compounds in phosphate buffered saline (PBS, pH = 7.4). Both Dex-SA-RGD and Dex-SA-RGE formed transparent and clear solutions at the concentration of 5 mg/mL. When their concentration reached over 15 mg/mL, the opalescent hydrogel formed instantly in PBS solution without any external stimuli (Fig. 1A). Interestingly, as Dex-SA-RGD and Dex-SA-RGE dissolving into distilled water solution at 20 mg/mL, semitransparent solution were obtained (Fig. S3), implying that the ions in PBS solution is indispensable for hydrogelation. Unlike previously reported hydrogelation strategies, such as heating-cooling and enzymatic induction, this hydrogelation approach is gentle, facile, and controllable, endowing its great applicability in clinical practice.

3.2. Characterization

Owing to their amphiphilic characteristics, Dex-SA-RGD and Dex-SA-RGE can self-assemble in an aqueous solution, thus forming supramolecular aggregates or micelles, when their concentration is above the critical aggregate concentration (CAC). The CAC values of Dex-SA-RGD and Dex-SA-RGE were about 2.8 mM and 2.2 mM, respectively (Fig. 1B–C). This result indicates that Dex-SA-RGD and Dex-SA-RGE display a similar hydrophilic–lipophilic balance.

The secondary structures of Dex-SA-RGD and Dex-SA-RGE hydrogels were monitored by CD spectra. As shown in Fig. 1D, both Dex-SA-RGD and Dex-SA-RGE hydrogels have a negative band at about 190 nm and positive bands at 210 nm and 280 nm. The CD signals have a similar extended poly-L-prolin II-like conformation, indicating the formation of an extended helical conformation in hydrogel [46]. Additionally, in comparison with Dex-SA-RGD and Dex-SA-RGE hydrogels, the CD spectra of both Dex-SA-RGD and Dex-SA-RGE aqueous solution (50 μg/mL in distilled water solution) slightly changed (Fig. S4), implying that ion in PBS greatly influence the molecular arrangement during the hydrogelation.

To investigate the viscoelastic properties of the hydrogels, we first performed the dynamic frequency sweeps of Dex-SA-RGD and Dex-SA-RGE hydrogels at 1% strain amplitude. The G′ values of both hydrogels were higher than G″ values at frequencies of 0.1–100 rad/s, indicating the formation of a relatively strong elastic network in the hydrogels (Fig. S5). It is worth noting that the proposed Dex-SA-RGD and Dex-SA-RGE hydrogels exhibited typical thixotropic behavior, i.e., hydrogels were broken down with the vortex or agitation, and the gel recovered immediately upon the withdrawal of the external strain. As reflected by the result of a step-strain experiment, both hydrogels collapsed into a quasi-liquid state as a result of a transition from low magnitude strain ($\gamma = 1\%$) to high magnitude strain ($\gamma = 100\%$), and the gel phase recovered immediately after the cessation of large magnitude strain ($\gamma = 100\%$) (Fig. 1E–F). This thixotropic property endows the proposed hydrogels to have great applicability in ophthalmic drug delivery, owing to the rapid gel-sol-gel transition during the intervals of physiological blinking.

To characterize the hydrogels composition after storage in different

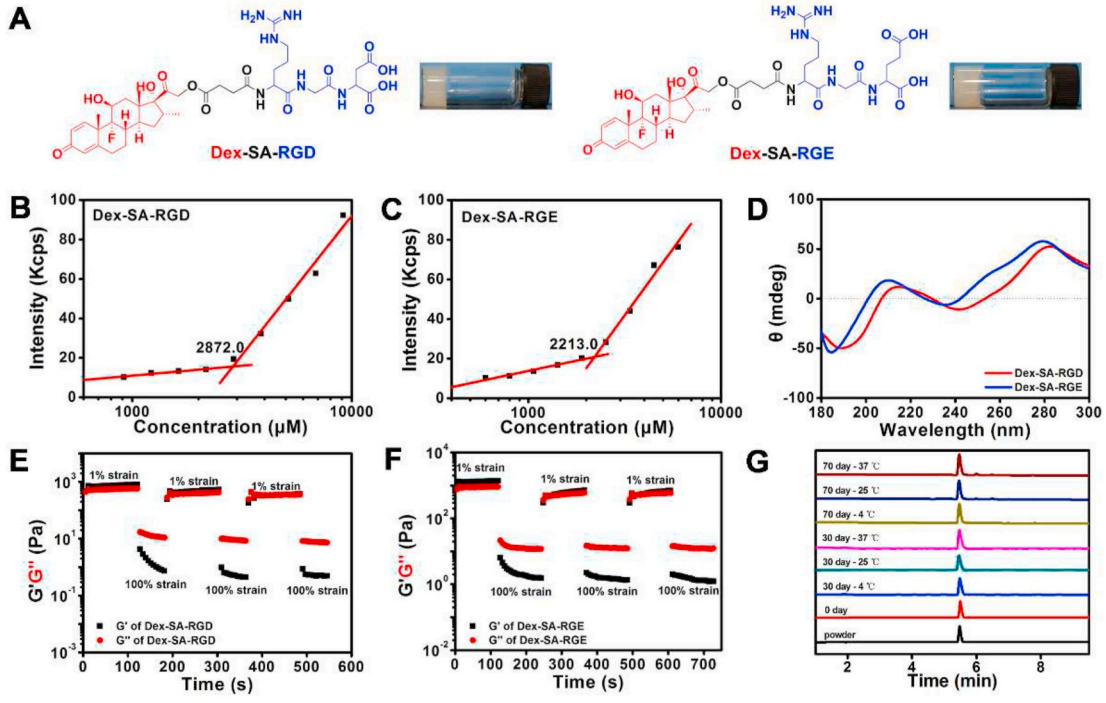

Fig. 1. (A) Chemical structure and appearance of Dex-SA-RGD/Dex-SA-RGE hydrogel (20 mg/mL Dex-SA-RGD or Dex-SA-RGE); **(B–C)** CAC value of Dex-SA-RGD and Dex-SA-RGE; **(D)** CD spectra of Dex-SA-RGD and Dex-SA-RGE hydrogel (20 mg/mL Dex-SA-RGD or Dex-SA-RGE) at room temperature; **(E–F)** A step-strain (1% and 100%) of Dex-SA-RGD and Dex-SA-RGE hydrogel (20 mg/mL Dex-SA-RGD or Dex-SA-RGE) at a frequency of 1 Hz; **(G)** HPLC traces of Dex-SA-RGD in powder and hydrogels after storage at 4 °C, 25 °C and 37 °C for 30 and 70 days.

conditions, the hydrogel samples were dissolved in methanol and the obtained solutions were injected into an HPLC system for analysis. As shown in Fig. 1G, Dex-SA-RGD did not undergo apparent hydrolysis during the hydrogelation, indicating the formation of a one-component supramolecular hydrogel. Even hydrogel storage at 4 °C, 25 °C, and 37 °C for 70 days did not cause apparent hydrolysis of Dex-SA-RGD (Fig. 1G). More importantly, Dex-SA-RGD supramolecular hydrogel could be lyophilized into a powder state for long-term storage. Upon the addition of an equal volume of distilled water, the hydrogel formed instantly (Fig. 2A). In addition, Dex-SA-RGD hydrogel displayed thermosensitive characteristics, i.e., the hydrogels turned into clear solutions as the temperature was above 45 °C, and the gelation occurred again after cooling down to room temperature (Fig. 2B–C).

We thereafter used transmission electron microscopy (TEM) to investigate the nature of the aggregates. As shown in Fig. 2D, for Dex-SA-RGD or Dex-SA-RGE aqueous solutions at 5 mg/mL, the vesicles have approached each other, forming "necklaces" like architecture. Similar phenomenon was also reported by Nicolae et al., who reported the formation of tubular vesicles by a tert-butylphenylamide derivative of cholic acid [47]. In the case of hydrogelation, the short nanotubes accompanied by helical ribbons were clearly observed at day 0 (Fig. S6). Uniform nanotubes formed for Dex-SA-RGD and Dex-SA-RGE hydrogels at 20 mg/mL with time extending to 14 days (Fig. 2 D). It is worth noting that the diameter of nanotubes from Dex-SA-RGD hydrogel (131.6 ± 2.2 nm) was about twice that of Dex-SA-RGE hydrogel (73.0 ± 4.7 nm). This result strongly indicates that the terminal amino acid of the drug-peptide conjugates remarkably affected the parallel arrangement of helical ribbons, thus influencing nanotubes formation.

3.3. In vitro release study

Numerous controlled drug release strategies have been proposed and described in the literature. Herein, we adopted a hydrolytically-mediated release approach to modulate the drug release behavior via covalent conjugation of the drug molecule through labile ester bond with biodegradable peptide sequence. As shown in Fig. 3A–B, the drug, in the form of Dex and its prodrug Dex-SA-RGD or Dex-SA-RGE, is rapidly released from the hydrogel accompanied by the dissolution of the hydrogel within 24 h. It seems to suggest that Dex-SA-RGD and Dex-SA-RGE underwent apparent ester bond hydrolysis as contacting with a large amount of phosphate buffered saline (PBS; pH = 7.4). Therefore, it is reasonable to believe that hydrolytically-mediated drug release from hydrogel is much more sensitive in the cellular microenvironment, owing to the existence of various esterase *in vivo*.

3.4. In vitro gel dissolution in artificial tears

In order to evaluate the resistance of tear elimination by the proposed Dex-SA-RGD hydrogel, we thereafter monitored the dissolution rate of hydrogel after incubation with artificial tears in an air bath (37 ± 0.2 °C). As presented in Fig. S7, the hydrogel was eroded gradually within 60min, suggesting the rapid dissolution of hydrogel in artificial tears. This result might be attributed to the relatively good solubility of Dex-SA-RGD in artificial tears. On other hand, the Dex-SA-RGD hydrogel might be able to provide a relatively longer precorneal retention via the resistance of tear elimination over than conventional eye drop formulation.

3.5. In vitro cytotoxicity and anti-inflammatory effects

Before anti-inflammatory assays, an MTT assay was utilized to assess the cytotoxicity of Dex-SA-RGD and Dex-SA-RGE on HCEC cells and RAW264.7 macrophages after 24 h of incubation. Fig. 3C–D shows that, up to 100 μM, both compounds did not induce apparent cytotoxicity in these two cell lines. This result was in accordance with the report of a previous study that, at a low dose, Dex only regulated the gene transcription but did not influence the survival of inflammatory cells [48]. Then the anti-inflammatory effect of Dex-SA-RGD on the RAW 264.7 macrophages was investigated, using Dex-SA-RGE as a control compound (Fig. 3E–G). After contact with LPS, cytokines, including nitrite, TNF-α, and IL-6 in cell culture medium, elevated significantly. Conversely, Dex-SA-RGD, and Dex-SA-RGE at 200 nM remarkably reduced the LPS-induced production of nitrite, TNF-α, and IL-6. It is worth noting that the inhibitory effect of Dex-SA-RGD is superior over that of Dex-SA-RGE, owing to the enhanced cellular uptake mediated by the RGD motif.

Nuclear factor κB (NF-κB) is a very important heterodimeric transcription factor that is responsible for inflammatory and immune response. We thereafter investigated whether NF-κB signaling is involved in the enhanced anti-inflammatory efficacy mediated by Dex-SA-RGD. As shown in Fig. 4 A, western blotting analyses revealed that LPS activation elevated significantly phosphorylation of p65 and IκB as compared to the control. Following treatment by Dex-SA-RGD or Dex-SA-RGE, LPS-induced phosphorylation of p65 and IκB were significantly attenuated. It is worth noting that Dex-SA-RGD displayed more potent inhibitory effect on the phosphorylation of p65 and IκB over than Dex-SA-RGE did. This might be attributed to the fact that more Dex was uptake by cells mediated by the RGD motif. We further used immunofluorescence analysis to assess the NF-κB activity according to the nuclear translocation of the p65 subunit of NF-κB. As presented in Fig. 4 B, LPS activation remarkably increased p65 nuclear translocation as compared to the control. As expected, LPS-induced p65 nuclear

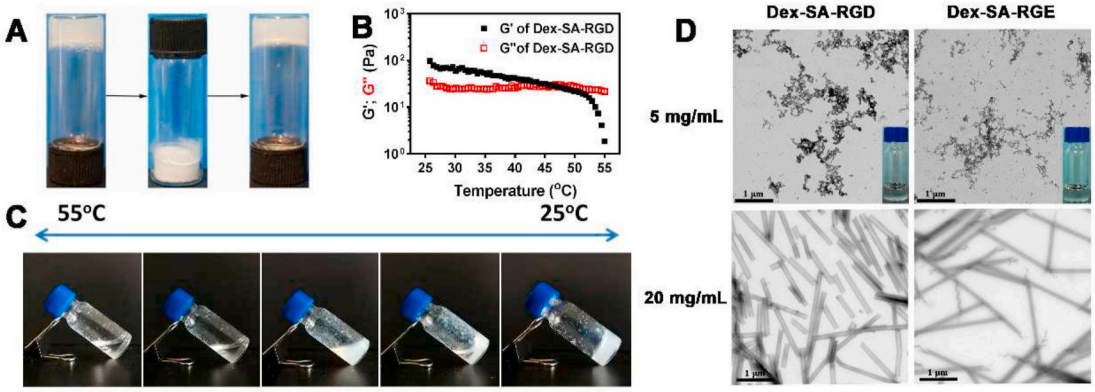

Fig. 2. (A) The rehydration of lyophilized Dex-SA-RGD hydrogel at 20 mg/mL ; **(B)** Temperature sweeps to assess the viscoelastic characteristics of Dex-SA-RGD hydrogel at 20 mg/mL; **(C)** Phase transition of Dex-SA-RGD hydrogel (20 mg/mL) as function with temperature; **(D)** TEM images of Dex-SA-RGD/Dex-SA-RGE solution (5 mg/mL) and Dex-SA-RGD/Dex-SA-RGE hydrogel (20 mg/mL) formed at 14th day.

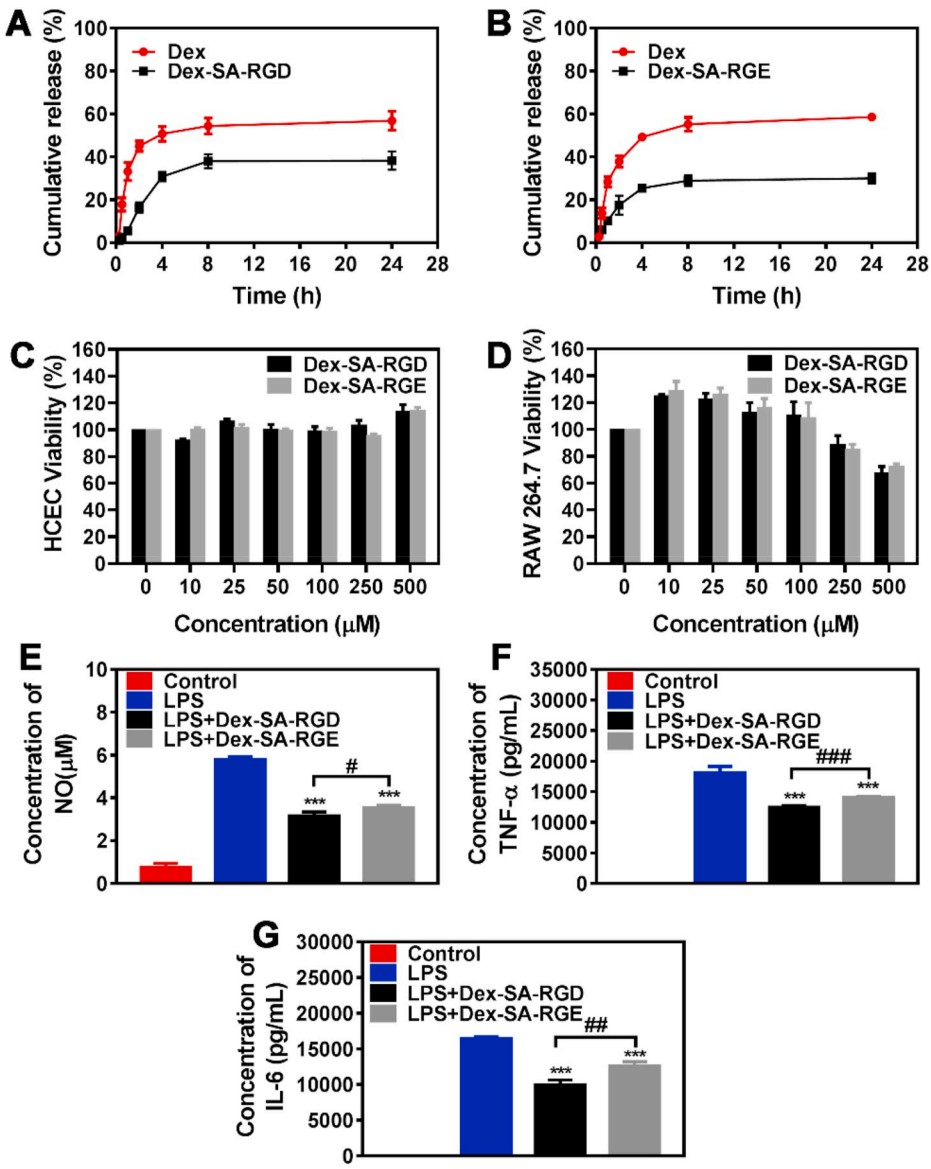

Fig. 3. *In vitro* drug release of Dex and Dex-SA-RGD/Dex-SA-RGE from **(A)** 20 mg/mL Dex-SA-RGD hydrogel and **(B)** 20 mg/mL Dex-SA-RGE hydrogel in PBS (pH = 7.4) at 37 °C; *In vitro* cytotoxicity of Dex-SA-RGD **(C)** and Dex-SA-RGE **(D)** against HCECs and RAW 264.7 macrophages after 24 h incubation; **(E)** NO, **(F)** IL-6 and **(G)** TNF-α levels in cell culture medium after treatment with 200 nM Dex-SA-RGD and Dex-SA-RGE in LPS-activated RAW 264.7 macrophages. $^{***}P < 0.001$ *vs.* LPS-activated group; $^{\#}P < 0.05$, $^{\#\#}P < 0.01$, and $^{\#\#\#}P < 0.001$ *vs.* Dex-SA-RGD-treated group.

translocation was dramatically inhibited by Dex-SA-RGD or Dex-SA-RGE treatment, and the Dex-SA-RGD treatment exhibited a more potent capacity to reduce the p65 nuclear translocation over than Dex-SA-RGE treatment. Our work documented that the boosting anti-inflammatory efficacy induced by the Dex-SA-RGD are primarily associated with NF-κB signaling inhibition.

3.6. Cellular uptake assay

To evaluate the cell-penetration of Dex-SA-RGD, we adopted Dex-SA-RGE as a control compound for cellular uptake evaluation *in vitro*. The time-dependent uptake of Dex-SA-K(NBD)RGD and Dex-SA-K(NBD)RGE in HCEC cells was investigated at 0.5 and 2 h using a confocal microscope. As shown in Fig. 5, the blue nuclei were surrounded by green fluorescence in the cells treated by Dex-SA-K(NBD)RGD after 2 h of incubation, while almost no visible green fluorescence was observed in the cells treated by Dex-SA-K(NBD)RGE after 2 h of incubation. This result implies that the cellular uptake occurred through active transport mediated by the RGD motif. To further verify this view, the cells were pre-incubated with Dex-SA-RGD to block the integrins, then co-cultured with Dex-SA-K(NBD)RGD for 0.5 and 2 h. The fluorescence intensity decreased significantly as compared with that caused by Dex-SA-K(NBD) RGD treatment alone, further indicating that RGD modification had increased performance in terms of integrin targeting and cellular uptake.

3.7. Corneal distribution

Although the *in vitro* cellular uptake results obtained for Dex-SA-K(NBD)RGD are promising, only *in vivo* experiments can truly evaluate the influence of physiological mechanisms such as tear drainage and eye blinking. To study the transcorneal distribution of Dex-SA-K(NBD)RGD and Dex-SA-K(NBD)RGE after topical instillation, we prepared frozen sections of the whole eyeball, and then observed the cornea using an inverted fluorescence microscope (Fig. 6). The green fluorescent signals of Dex-SA-K(NBD)RGE were primarily concentrated in the corneal epithelium 15 min after topical instillation. In regard to Dex-SA-K(NBD)RGD, obvious green fluorescence signals were observed in the entire corneal architecture (epithelium, stroma, and endothelium) at 15 min after topical instillation, demonstrating rapid transcorneal penetration and distribution, which might be due to the active transport mediated by RGD-integrin interaction. After 45-min exposure, the green fluorescence signals of Dex-SA-K(NBD)RGE decayed significantly and failed to penetrate inside the cornea. Conversely, Dex-SA-K(NBD)RGD exhibited a more profound green fluorescence signal and deeper transmission into

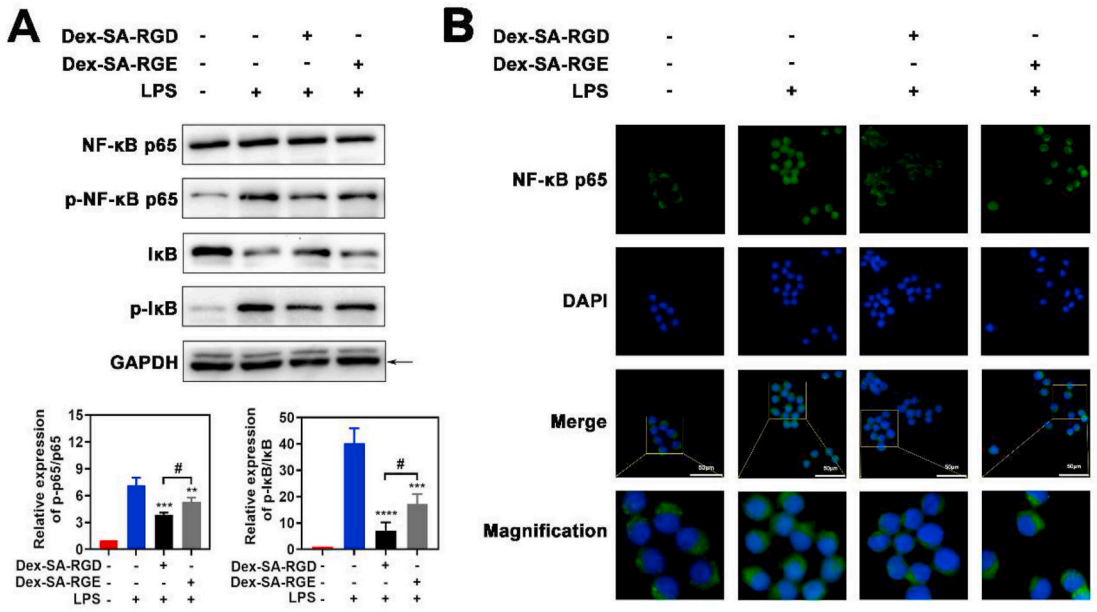

Fig. 4. Des-SA-RGD showed more potent capacity on the NF-κB signaling inhibition towards LPS-activated RAW264.7 macrophages. **(A)** Western blotting analysis of p-IκB and p-p65 proteins in RAW264.7 macrophages. **P < 0.01, ***P < 0.001, and ****P < 0.0001 *vs.* LPS-activated group. #P < 0.05 *vs.* Dex-SA-RGD-treated group. **(B)** Fluorescence microscopy images of RAW264.7 macrophages. Cell nuclei are shown in blue and p65 is shown in green. Scale bar: 50 μm.

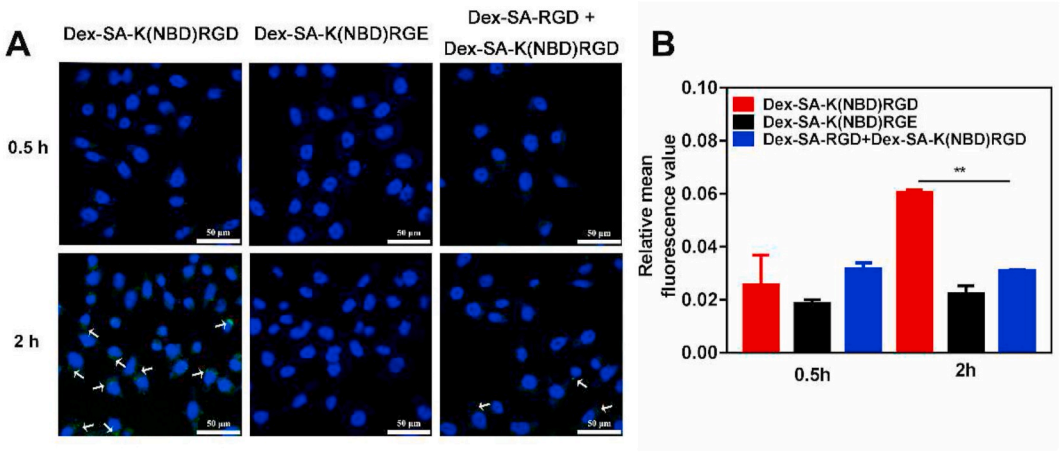

Fig. 5. (A) Cellular uptake of Dex-SA-K(NBD)RGD and Dex-SA-K(NBD)RGE (500 μM) evaluated by confocal microscopy after 0.5 and 2 h of incubation. Cells were pre-treated by 500 μM Dex-SA-RGD for 2 h, and then incubated with 500 μM Dex-SA-K(NBD)RGD for 0.5 and 2 h to visualize the fluorescence signal. Scale bar: 50 μm. **(B)** Relative mean fluorescence value of cells; **p < 0.01 *vs* Dex-SA-RGE and Dex-SA-RGD + Dex-SA-K(NBD)RGD.

the entire cornea 45 min after topical instillation. These results strongly support the concept that precorneal retention and transcorneal permeability of drugs could be effectively enhanced after being mediated by the RGD motif.

4. Conclusion

In conclusion, we report a drug-peptide supramolecular hydrogel based on anti-inflammatory drug, dexamethasone (Dex), and Arg-Gly-Asp (RGD) motif for topical ocular drug delivery. The drug-peptide supramolecular hydrogel formed spontaneously in phosphate buffered saline (PBS, pH = 7.4) without external stimuli. In comparison with Dex-SA-RGE, the Dex-SA-RGD exhibited a more potent *in vitro* anti-inflammatory efficacy in lipopolysaccharide (LPS)-activated RAW 264.7 macrophages via the inhibition of nuclear factor κB (NF-κB) signal pathway. Using NBD-labeled drug-peptide supramolecular hydrogel, the Dex-SA-K(NBD)RGD showed increased performance in terms of integrin targeting and cellular uptake compared to Dex-SA-K(NBD)RGE, as revealed by cellular uptake assay. On topical instillation, the proposed Dex-SA-K(NBD)RGD could effectively enhance the precorneal retention and transcorneal permeability with respect to the Dex-SA-K(NBD)RGE. Overall, we believe this study will be useful for the design of a novel ophthalmic drug delivery approach to boost drug transcorneal permeability and pharmacological activity by establishing ligand-receptor pairs.

CRediT authorship contribution statement

Lin Chen: Data curation, Writing – original draft. **Jie Deng:** Conceptualization, Methodology, Writing – review & editing. **Ailing Yu:** Data curation, Writing – original draft. **Yuhan Hu:** Data curation, Writing – original draft. **Bo Jin:** Software, Visualization, Investigation. **Jianhong Zhou:** Software, Visualization, Investigation. **Lei Lei:** Software, Visualization, Investigation. **Yuan Wang:** Software, Visualization,

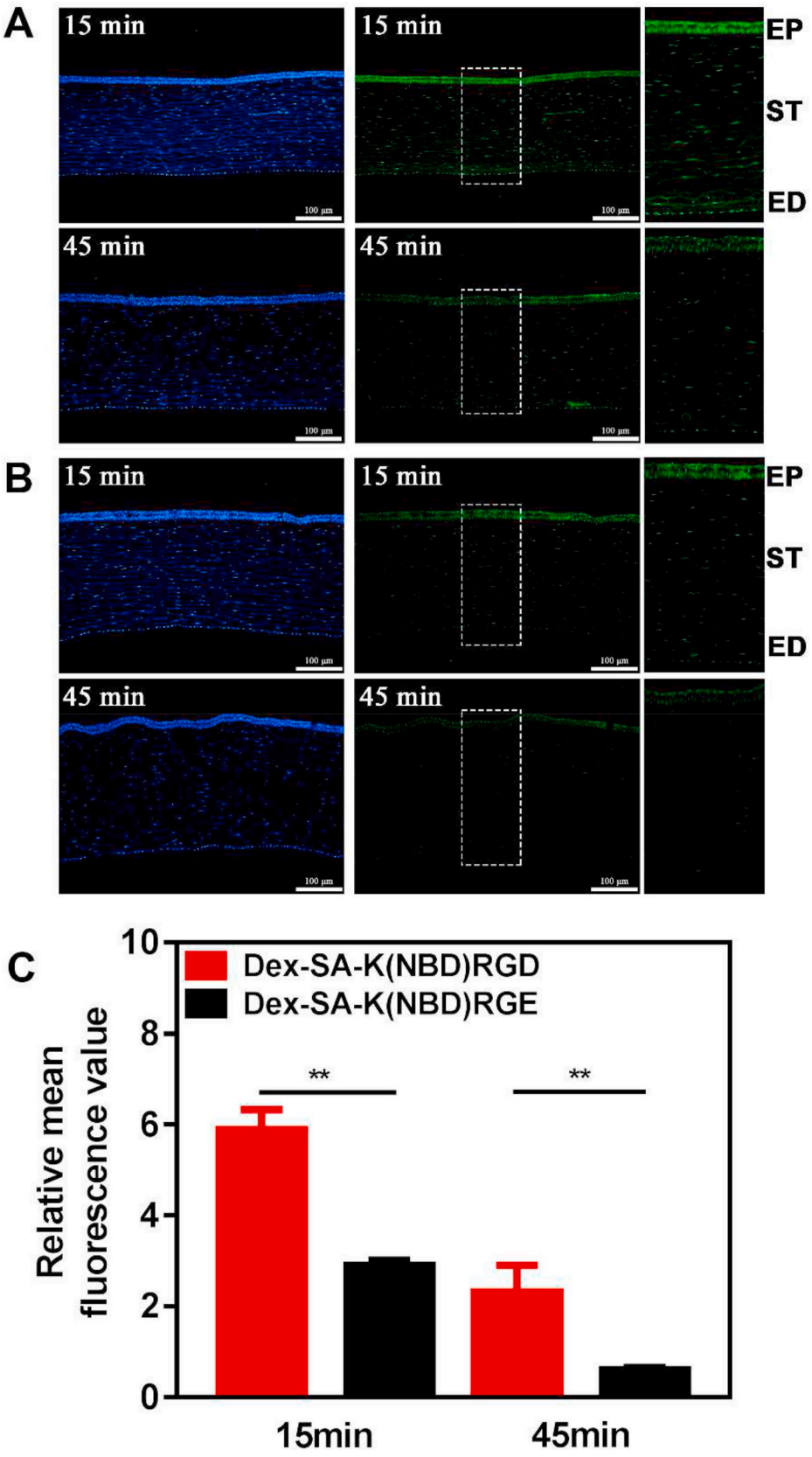

Fig. 6. Fluorescence distribution after *in vivo* corneal permeation of **(A)** 20 mg/mL Dex-SA-K(NBD)RGD and **(B)** 20 mg/mL Dex-SA-K(NBD)RGE at 15 and 45 min post topical instillation. EP: Epithelium; ST: Stroma; ED: Endothelium. **(C)** Relative mean fluorescence value of cornea at 15 and 45 min post topical instillation. **p < 0.01.

Investigation. **Serhii Vakal:** Software, Visualization, Investigation, English editing. **Xingyi Li:** Conceptualization, Methodology, Writing – review & editing.

Declaration of competing interest

The authors declare that they have no known competing financial interests or personal relationships that could have appeared to influence the work reported in this paper.

Acknowledgments

This research was supported by the Zhejiang Provincial Natural Science Foundation of China (Grant No. LR18H300002 and LQ20C080002) and the National Natural Science Foundation of China (Grant No. 81971732).

Appendix A. Supplementary data

Supplementary data to this article can be found online at https://doi.org/10.1016/j.bioactmat.2021.09.006.

References

[1] G. Spaeth, J. Walt, J. Keener, Evaluation of quality of life for patients with glaucoma, Am. J. Ophthalmol. 141 (2006) 3–14.
[2] M.M. Liu, J. Tuo, C.-C. Chan, Gene therapy for ocular diseases, Br. J. Ophthalmol. 95 (2011) 604–612.
[3] P.M. Campos, R. Petrilli, R.F.V. Lopez, The prominence of the dosage form design to treat ocular diseases, Int. J. Pharm.. 586 (2020) 119577.
[4] A. Urtti, Challenges and obstacles of ocular pharmacokinetics and drug delivery, Adv. Drug Deliv. Rev. 58 (2006) 1131–1135.
[5] M.E. Myles, D.M. Neumann, J.M. Hill, Recent progress in ocular drug delivery for posterior segment disease: emphasis on transscleral iontophoresis, Adv. Drug Deliv. Rev. 57 (2005) 2063–2079.
[6] D. Huang, Y.-S. Chen, I.D. Rupenthal, Overcoming ocular drug delivery barriers through the use of physical forces, Adv. Drug Deliv. Rev. 126 (2018) 96–112.
[7] Y. Agban, S.S. Thakur, O.O. Mugisho, I.D. Rupenthal, Depot formulations to sustain periocular drug delivery to the posterior eye segment, Drug Discov. Today 24 (2019) 1458–1469.
[8] T. Meng, V. Kulkarni, R. Simmers, V. Brar, Q. Xu, Therapeutic implications of nanomedicine for ocular drug delivery, Drug Discov. Today 24 (2019) 1524–1538.
[9] S. Gorantla, V.K. Rapalli, T. Waghule, P.P. Singh, S.K. Dubey, R.N. Saha, G. Singhvi, Nanocarriers for ocular drug delivery: current status and translational opportunity, RSC Adv. 10 (2020) 27835–27855.
[10] D. Liu, B. Wan, J. Qi, X. Dong, W. Zhao, W. Wu, Y. Dai, Y. Lu, Z. Chen, Permeation into but not across the cornea: bioimaging of intact nanoemulsions and nanosuspensions using aggregation-caused quenching probes, Chin. Chem. Lett. 29 (2018) 1834–1838.
[11] M. Dubald, S. Bourgeois, V. Andrieu, H. Fessi, Ophthalmic drug delivery systems for antibiotherapy- review, Pharmaceutics 10 (2018) 10.
[12] A.A. Al-Kinani, G. Zidan, N. Elsaid, A. Seyfoddin, A.W.G. Alani, R.G. Alany, Ophthalmic gels: past, present and future, Adv. Drug Deliv. Rev. 126 (2018) 113–126.
[13] H. Shi, Y. Wang, Z. Bao, D. Lin, H. Liu, A. Yu, L. Lei, X. Li, X. Xu, Thermosensitive glycol chitosan-based hydrogel as a topical ocular drug delivery system for enhanced ocular bioavailability, Int. J. Pharm.. 570 (2019), 118688.
[14] A. Nieto, H. Hou, M.J. Sailor, W.R. Freeman, L. Cheng, Ocular silicon distribution and clearance following intravitreal injection of porous silicon microparticles, Exp. Eye Res. 116 (2013) 161–168.
[15] A. Yu, H. Shi, H. Liu, Z. Bao, M. Dai, D. Lin, D. Lin, X. Xu, X. Li, Y. Wang, Mucoadhesive dexamethasone-glycol chitosan nanoparticles for ophthalmic drug delivery, Int. J. Pharm.. 575 (2020) 118943.
[16] M.A.B. Henostroza, K.J.C. Melo, M.N. Yukuyama, R. Löbenberg, N.A. Bou-Chacra, Cationic rifampicin nanoemulsion for the treatment of ocular tuberculosis, Colloid. Surface. (2020), 124755.
[17] N. Elsaid, T.L. Jackson, Z. Elsaid, A. Alqathama, S. Somavarapu, PLGA microparticles entrapping chitosan-based nanoparticles for the ocular delivery of ranibizumab, Mol. Pharm. 13 (2016) 2923–2940.
[18] E. Korhonen, S. Rönkkö, S. Hillebrand, J. Riikonen, W. Xu, K. Järvinen, V.-P. Lehto, A. Kauppinen, Cytotoxicity assessment of porous silicon microparticles for ocular drug delivery, Eur. J. Pharm. Biopharm. 100 (2016) 1–8.
[19] Y. Zhou, A. Fang, F. Wang, H. Li, Q. Jin, L. Huang, C. Fu, J. Zeng, Z. Jin, X. Song, Core-shell lipid-polymer nanoparticles as a promising ocular drug delivery system to treat glaucoma, Chin. Chem. Lett. 31 (2020) 494–500.
[20] V.K. Yellepeddi, S. Palakurthi, Recent advances in topical ocular drug delivery, J. Ocul. Pharmacol. Therapeut. 32 (2016) 67.
[21] D. Lin, L. Lei, S. Shi, X. Li, Stimulus-responsive hydrogel for ophthalmic drug delivery, Macromol. Biosci. 19 (2019), 1900001.
[22] E. Bellotti, M.V. Fedorchak, S. Velankar, S.R. Little, Tuning of thermoresponsive pNIPAAm hydrogels for the topical retention of controlled release ocular therapeutics, J. Mater. Chem. B 7 (2019) 1276–1283.
[23] A. Sun, X. He, X. Ji, D. Hu, M. Pan, L. Zhang, Z. Qian, Current research progress of photopolymerized hydrogels in tissue engineering, Chin. Chem. Lett. 32 (2021) 2117–2126.
[24] J. Ceulemans, A. Ludwig, Optimisation of carbomer viscous eye drops: an in vitro experimental design approach using rheological techniques, Eur. J. Pharm. Biopharm. 54 (2002) 41–50.
[25] A. Rozier, C. Mazuel, J. Grove, B. Plazonnet, Functionality testing of gellan gum, a polymeric excipient material for ophthalmic dosage forms, Int. J. Pharm.. 153 (1997) 191–198.
[26] Y. Wang, A.G. Cheetham, G. Angacian, H. Su, L. Xie, H. Cui, Peptide-prug conjugates as effective prodrug strategies for targeted delivery, Adv. Drug Deliv. Rev. 110 (2017) 112–126.
[27] C. Liang, L. Zhang, W. Zhao, L. Xu, Y. Chen, J. Long, F. Wang, L. Wang, Z. Yang, Supramolecular nanofibers of drug-peptide amphiphile and affibody suppress HER2+ tumor growth, Adv. Healthc. Mater. 7 (2018), 1800899.
[28] X. Du, J. Zhou, J. Shi, B. Xu, Supramolecular hydrogelators and hydrogels: from soft matter to molecular biomaterials, Chem. Rev. 115 (2015) 13165–13307.
[29] R. Lin, H. Cui, Supramolecular nanostructures as drug carriers, Curr. Opin. Chem. Eng. 7 (2015) 75–83.
[30] W. Ma, A.G. Cheetham, H. Cui, Building nanostructures with drugs, Nano Today 11 (2016) 13–30.
[31] S. Sundar, Y. Chen, Y.W. Tong, Delivery of therapeutics and molecules using self-assembled peptides, Curr. Med. Chem. 21 (2014) 2469–2479.
[32] C. Yang, Z. Wang, C. Ou, M. Chen, L. Wang, Z. Yang, A supramolecular hydrogelator of curcumin, Chem. Commun. 50 (2014) 9413–9415.
[33] T. Nishida, M. Inui, M. Nomizu, Peptide therapies for ocular surface disturbances based on fibronectin-integrin interactions, Prog. Retin. Eye Res. 47 (2015) 38–63.
[34] H. Guo, G. Du, L. Wang, D. Wang, L. Hu, Y. Huang, Integrin alpha v beta 6 contributes to maintaining corneal epithelial barrier function, Cell Biol. Int. 37 (2013) 593–599.
[35] M.A. Stepp, S. Spurr-Michaud, I.K. Gipson, Integrins in the wounded and unwounded stratified squamous epithelium of the cornea, Invest. Ophthalmol. Vis. Sci. 34 (1993) 1829–1844.
[36] M.A. Stepp, Corneal integrins and their functions, Exp. Eye Res. 83 (2006) 3–15.
[37] C. Gong, S. Shi, P. Dong, B. Kan, M. Gou, X. Wang, X. Li, F. Luo, X. Zhao, Y. Wei, Synthesis and characterization of PEG-PCL-PEG thermosensitive hydrogel, Int. J. Pharm.. 365 (2009) 89–99.
[38] C. Liang, X. Yan, R. Zhang, T. Xu, D. Zheng, Z. Tan, Y. Chen, Z. Gao, L. Wang, X. Li, Z. Yang, Enhanced cellular uptake and nuclear accumulation of drug-peptide nanomedicines prepared by enzyme-instructed self-assembly, J. Contr. Release 317 (2020) 109–117.
[39] P. Zheng, Y. Liu, J. Chen, W. Xu, G. Li, J. Ding, Targeted pH-responsive polyion complex micelle for controlled intracellular drug delivery, Chin. Chem. Lett. 31 (2020) 1178–1182.
[40] F. Chogan, T. Mirmajidi, A.H. Rezayan, A.M. Sharifi, A. Ghahary, J. Nourmohammadi, A. Kamali, M. Rahaie, Design, fabrication, and optimization of a dual function three-layer scaffold for controlled release of metformin hydrochloride to alleviate fibrosis and accelerate wound healing, Acta Biomater. 113 (2020) 144–163.
[41] A.E. Stanton, X. Tong, F. Yang, Extracellular matrix type modulates mechanotransduction of stem cells, Acta Biomater. 96 (2019) 310–320.
[42] X. Pu, X. Zhou, Z. Huang, G. Yin, X. Chen, Fabrication of extracellular matrix-coated conductive polypyrrole-poly (l-lactide) fiber-films and their synergistic effect with (nerve growth factor)/(epidermal growth factor) on neurites growth, Chin. Chem. Lett. 31 (2020) 1141–1146.
[43] N.C. Hunt, D. Hallam, A. Karimi, C.B. Mellough, J. Chen, D.H.W. Steel, M. Lako, 3D culture of human pluripotent stem cells in RGD-alginate hydrogel improves retinal tissue development, Acta Biomater. 49 (2017) 329–343.
[44] K.-M. Lee, J.-H. Kim, E.-S. Choi, E. Kim, S.-K. Choi, W.B. Jeon, RGD-containing elastin-like polypeptide improves islet transplantation outcomes in diabetic mice, Acta Biomater. 94 (2019) 351–360.
[45] R. Zhang, L. Xie, H. Wu, T. Yang, Q. Zhang, Y. Tian, Y. Liu, X. Han, W. Guo, M. He, Alginate/laponite hydrogel microspheres co-encapsulating dental pulp stem cells and VEGF for endodontic regeneration, Acta Biomater. 113 (2020) 305–316.
[46] N.J. Greenfield, Using circular dichroism spectra to estimate protein secondary structure, Nat. Protoc. 1 (2006) 2876.
[47] V.H. Soto Tellini, A. Jover, F. Meijide, J. Vazquez Tato, L. Galantini, N.V. Pavel, Supramolecular structures generated by ap-tert-Butylphenyl-amide derivative of cholic acid: from vesicles to molecular tubes, Adv. Mater. 19 (2007) 1752–1756.
[48] M. Zen, M. Canova, C. Campana, S. Bettio, L. Nalotto, M. Rampudda, R. Ramonda, L. Iaccarino, A. Doria, The kaleidoscope of glucorticoid effects on immune system, Autoimmun. Rev. 10 (2011) 305–310.